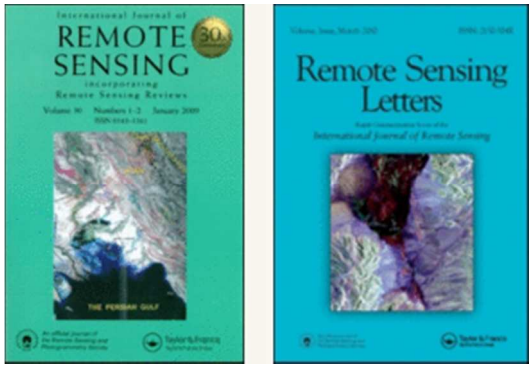

Evaluation of satellite based dust detection algorithms in the Middle East region

Journal:	*International Journal of Remote Sensing*
Manuscript ID	TRES-PAP-2017-1043.R2
Manuscript Type:	IJRS Research Paper
Date Submitted by the Author:	16-Apr-2018
Complete List of Authors:	Bin abdulwahed, Abdullah; University of Southampton, Geography and Environment Dash, Jadunandan; University of Southampton, Geography and Environment Roberts, Gareth; University of Southampton, Geography and Environment
Keywords:	aerosols, aeronet, Dust storm, MODIS
Keywords (user defined):	Earth Observation, Middle East

Evaluation of satellite dust detection algorithms in the Middle East region

Abdullah bin Abdulwahed*, Jadunandan Dash and Gareth Roberts

Geography and Environment, University of Southampton, Southampton, United Kingdom

Abdullah bin Abdulwahed, aba1g11@soton.ac.uk

Prof. Jadunandan Dash, J.Dash@soton.ac.uk

Dr. Gareth Roberts, G.J.Roberts@soton.ac.uk

Abstract

In recent years, the frequency, spatial extent and intensity of dust storms has increased and it is one of the main continuously occurring environmental hazard in the Middle East region. Since dust storms generally cover a large spatial extent and are highly dynamic, satellite Earth Observation is a key tool for detecting their occurrence, identifying their origin and monitoring their transport and state. A variety of satellite dust detection algorithms have been developed to identify dust emissions sources and dust plumes once entrained in the atmosphere. This paper evaluates the performance of five widely applied dust detection algorithms: the Brightness Temperature Difference (BTD), D-parameter, Normalized Difference Dust Index (NDDI), Thermal-Infrared Dust Index (TDI) and the Middle East Dust Index (MEDI). These algorithms are applied to MODIS (MOD21KM) data to detect dust-contaminated pixels during three significant dust events in 2007 in the Middle East region that originated from sources in Iraq, Syria and Saudi Arabia. The results indicate that all methods have a comparable performance in detecting dust-contaminated pixels during the three dust events with an average detection rate (between all algorithms) of 85%. However, substantial differences exist in their ability to distinguish dust from clouds and the land surface, which resulted in large errors of commission. Direct validation of these algorithms with observations from seven Aerosol Robotic Network (AERONET) stations in the region found an average false detection rate (between all algorithms) of 89.6%. Although the algorithms performed well in detecting the dust contaminated pixels their high false detection rate means it is challenging to apply these algorithms in operational context.

Keywords: Dust Detection; Earth Observation; MODIS; Middle East; AERONET

1. Introduction

Dust storms, often-referred to as meteorological phenomena, are commonly experienced in the arid, semi-arid and related environments (Goudie and Middleton 2006). They occur when a strong winds blow through these environments and entrain loose particles, transporting them large distances via saltation and suspension (Shao 2008). Dust storms can affect large areas with dust being transported thousands of kilometres over short periods of time. For example, studies have shown that Saharan dust has been transported to the Americas (Ben-

Ami et al. 2010), Europe (Varga et al. 2013), the Near East (Thevenon et al. 2011) and the Arctic (Barkan and Alpert 2010). In over most of the Middle East and Northern Africa region, there has been a significant increase in the frequency and the intensity of dust storms over the past 15 years (Stanelle et al. 2014).

The increasing frequency of dust storms is often an early warning of land degradation which may result from poor land management practices and the increasing conversion of savanna to agricultural land (Natsagdorj, Jugder, and Chung 2003; Laurent 2005; Tegen et al. 2004). Ginoux et al. (2012) estimated that, between 2003 to 2009, the total annual global dust emissions was 1536 Tg and that 25% was attributable to anthropogenic sources (e.g. agriculture). To compound this issue, drought and arid conditions favour the dissolution of dust particles leading to increasing dust emissions (Arimoto 2001; Goudie and Middleton 2006).

The social and environmental effects from dust storms are wide ranging and affect the source, transport and deposition environments. In the source region, dust storms result in the loss of topsoil which reduces soil fertility, increases soil erosion and accelerates land degradation and desertification (Tozer and Leys 2013). However, it is during dust transportation in the atmosphere that the most pronounced effects are evident. The reduction of visibility can lead to the closure of schools and businesses and can hinder road and air transportation; all of which result in economic loss (Crooks and Cowan 1993; Pauley et al. 1996; Kim et al. 2001; Chung et al. 2003). Dust events also have health implications as the atmospheric concentration of particulate matter (PM) can exceed the World Health Organization (WHO) guideline for PM10 (50 μg/m3) for a 24-hr mean during dust storm events (Ozer et al. 2007; Chu et al. 2008; Brunekreef and Forsberg 2005). Under these conditions, dust storms can have severe consequences for those affected by respiratory illness and asthma (Bener et al. 1996) which can be exacerbated further if the dust emissions contain

chemicals such as fungi, bacteria, herbicides, salts, and fine particles (Kellogg and Griffin 2006; Small et al. 2001).

Dust properties are frequently measured using ground-based observations using Sun photometers such as those in the Aerosol Robotic Network (AERONET; Dubovik and King 2000). The AERONET network provides high temporal resolution aerosol optical depth (AOD) measurements have been widely applied for dust loadings and transport routes studies (Sun et al. 2001; Zhang et al. 2003; Darmenova and Sokolik 2005). However, ground observations have limited spatial coverage and this has led to the application of Earth Observation (EO) for monitoring dust events. Due to their spatio-temporal characteristics, EO data has become one of the most commonly used approaches to detect and map dust events (Hansell et al. 2007; Baddock et al. 2009; Vickery et al. 2013). EO imagery from Meteosat (Legrand et al. 2001; Moorthy et al. 2007), MISR (Prasad and Singh 2007; Tesfaye et al. 2011; Rashki et al. 2013), Advanced Very High Resolution Radiometer (AVHRR; Cakmur, Miller and Tegen 2001; Zhu et al. 2007), Sea-viewing Wide Field-of-view Sensor (SeaWiFS; Fischer et al. 2009; Mélin et al.2010), Total Ozone Mapping Spectrometer (TOMS; El-Askary et al. 2006; Rashki et al. 2013) and MODIS (Karimi et al. 2012; Sayer et al. 2013; Liu and Liu 2015; O'Loingsigh et al. 2015) have been used to detect dust events over different regions.

The main challenge in detecting dust using satellite data concerns effective separation of the spectral signal of atmospheric dust from that of the land surface and cloud and this is particularly challenging over bright surfaces using the visible and near infrared wavelengths (Hsu et al. 2004, 2006; Rashki et al. 2013). However, dust has a unique radiative signature in the longwave infrared (LWIR) region which results in a reduction of temperature with increasing wavelength (Ackerman 1997). This characteristic has been exploited to separate dust from other aerosols through the development of Brightness Temperature Difference

(BTD) based algorithms that utilise the temperature difference between principally the 10μm and 11μm LWIR wavebands. The BTD approach has been successfully applied for detecting dust using EO data. According to Ackerman (1997), the BTD between 8.5, 11 and 12μm wavelengths is suitable for detecting dust aerosol over land and ocean. However, the magnitude or the sign of the BTD is affected by the dust mineral composition, dust layer height, and the surface emissivity which affects the ability to detect dust in different regions without adjusting the thresholds (Darmenov and Sokolik 2005). The most common method of detecting dust events is via spectral indices as these are easily to apply and utilise spectral wavebands available on most satellite sensors. Through the analysis of spectral signatures of dust aerosols over a wide range of wavelengths, various dust detection indices have been developed to separate dust from clouds, underlying surface and clear scenes (Roskovensky and Liou 2005; Qu et al. 2006). Some methods use visible channels (Qu et al. 2006), while some indices use both visible and thermal wavebands to separate dust from clouds (Roskovensky and Liou 2005). However, spectral indices can be subjective and they are somewhat dependant on the instrument spatial and spectral resolution (Benedetti et al. 2014) and the heterogeneity of the underlying land surface (Samadi et al. 2014); there are these algorithms are often limited to the areas where there were developed and often prohibit their application at a regional to global scale.

The purpose of this study is to assess the ability of five commonly used dust spectral indices which include the Brightness Temperature Difference (BTD; Ackerman 1997), D-parameter (Roskovensky and Liou 2005), Normalized Difference Dust Index (NDDI; Qu et al. 2006), Thermal-Infrared Dust Index (TDI; Hao and Qu 2007) and the Middle East Dust Index (MEDI; Karimi et al. 2012) to detect dust events over the Middle East region. This region was selected as it is frequently impacted by dust storms and it believed to contribute to between 11 and 28% of the annual global dust production, which equates to between 221 and

496 Tg dust (Hamidi et al. 2013; Zender et al. 2003; Ginoux et al. 2004; Tanaka et al. 2006). In comparison, the Bodélé Depression in northern Chad is estimated to be responsible for between 6–18% of global dust emissions (Todd et al. 2007). These algorithms were applied to level 1B MODIS images over three dust events in the Middle East to evaluate their performance across the region. The three case studies were chosen to illustrate main types of events that occur in the Middle East region, and to include factors that can significantly affect dust plume identification such as their seasonality and the dust source origin. These algorithms were also applied to one-year dataset of MODIS imagery (MO/YD21KM) and the frequency of dust detection was compared with ground-based AOD measurements from seven AERONET sites in the Middle East.

The remainder of this paper is organized as follows: study area and description of used datasets are given in section 2. Section 3 briefly describes the five dust detection algorithms. In section 4, the dust detection performance of the algorithms is validated using AERONET data. Section 5 discusses the application and evaluation these algorithms whilst sections 6 and 7 are the discussion and conclusion.

2. Materials and methods

2.1. *Study Area*

The climate in the Middle East is consistent throughout the year with little rainfall and limited seasonal or geographic variation (Zhang et al. 2005). Approximately 60% of the regions rainfall occurs between October and March as a result of Indian Ocean monsoon (Abdullah and Al-Mazroui 1998). The region is home to the worlds largest desert, the Rub al Khali, which measures 582,750 km and covers much of the Southern interior of the Arab Peninsula (Goudie 2013). The scarce and erratic rainfall and varying temperatures combined to shape the distribution and abundance of the scarce vegetation cover (Boer 1997; Kadioglu

and Saylan 2001). These factors, coupled with the vulnerability to soil erosion, contribute to the increasing frequency of dust storms in the region. In some seasons and for approximately 30% of the time, on average, parts of the Middle East, particularly the kingdom Saudi Arabia, are affected by dust events (Maghrabi et al, 2011). Most dust storms occur during spring and summer months due to the climatic conditions associated with strong, hot and dry winds (Prospero and Carlson 1981; Middleton 1986; Kutiel and Furman 2003). Dust activity starts in March and April, peaks in June and July and the month of September on the other side faces less dust storms (Prospero et al. 2002). Even though, some of dust storms in the region originate from the Sahara, the Middle East region is considered a major source of dust. In this paper, three different dust events that originating from Iraq, Syria and Saudi Arabia are studied (Figure 1).

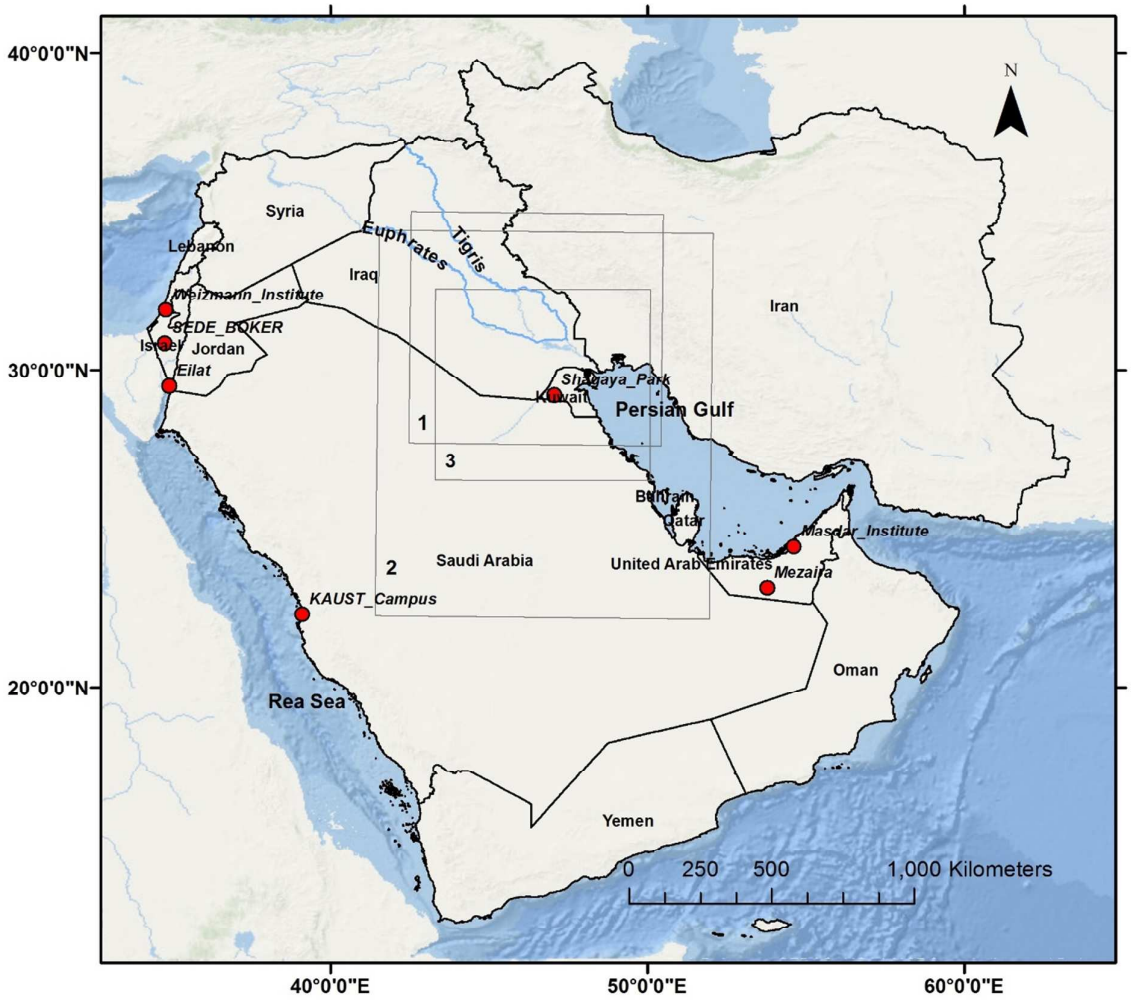

Figure 1.The study area and the coverage extents of the three dust events. Event 1: 5th February 2007, Event 2: 26th June 2007 and Event 3: 12th September 2007. Red points show the distribution of the seven AERONET stations used to validate the algorithms.

2.2 *Data set*

Here we used six MODIS Level 1B images from the Terra and Aqua satellites (three images for each) acquired on days with significant dust storm occurrence to assess five spectral dust indices (Table 1). Each event occurred in a different season and originated from a different dust source. In addition, the storms intensity, its spatial position in the imagery and the dust-affected areas are different in each event. To assist in the identification of dust-affected regions, daily MODIS Level 2 Aerosol Optical Depth (AOD) data (Kaufman et al. 1997;

Remer et al. 2005) were used to identify regions with high AOD. Cloud screening was achieved using the daily MODIS Level 2 Cloud Products (Platnick et al. 2015). Finally, the 500m MODIS Land Cover Type Product (MCD12Q1; Friedl et al. 2010) was used to assess the role of land cover type in the ability to detect dust. Although the MODIS land cover product has not been validated in the Middle East, its overall global accuracy is estimated to be 75% (Friedl et al. 2010). Validation of the dust detection algorithms is carried out using one-year of Terra and Aqua MODIS Level 1B data (2015) which are compared against AERONET AOD measurements from seven AERONET stations (Figure 1).

Table 1. Summary of the dust events that used for the seasonal evaluation of dust detection algorithms.

Event	Date	Data Type	Satellite (MOD/MYD) and overpass time (UTC)	Spatial resolution (km)
1	05/02/2007	MOD021/MYD021 (L1B)	(Terra)(07:20)/(Aqua)(10:30)	0.25, 0.5 and 1
		MOD04/MYD04 (AOD)		10 × 10
		MOD06/MYD06 (Cloud cover)		1
2	26/06/2007	MOD021/MYD021 (L1B)	(Terra)(06:50)/(Aqua)(10:00)	0.25, 0.5 and 1
		MOD04/MYD04 (AOD)		10 × 10
		MOD06/MYD06 (Cloud cover)		1
3	12/09/2007	MOD021/MYD021 (L1B)	(Terra)(07:00)/(Aqua)(10:10)	0.25, 0.5 and 1
		MOD04/MYD04 (AOD)		10 × 10
		MOD06/MYD06 (Cloud cover)		1
All	2007	MCD12Q1 (Land Cover)	MODIS Terra + Aqua Land Cover Type (Yearly)	0.5

3. Dust detection algorithm description

The following section describes the dust detection algorithms applied in this study which are commonly applied for global and regional dust detection:

A) The Ackerman (1997) algorithm is calculated using BTD of MODIS thermal band 31 ($BT11_{\mu m}$, 10.78–11.28 μm) and band 32 ($BT12_{\mu m}$, 11.77–12.27 μm) with the following formula:

$$\boldsymbol{BTD = (BT11_{\mu m} - BT12_{\mu m})} \quad (1)$$

Negative BTD values are indicative of dust (Ackerman 1997). Despite its simplicity, studies have also shown that the BTD varies regionally depending on the variability in surface emissivity and view zenith angle (Caquineau et al. 2002; Satheesh and Moorthy 2005). For seven regions, Darmenov and Sokolik (2005) examined the ability of the BTD algorithm to detect dust transported over water. They found that the dust detection threshold for the Nubian, Thar, Gobi/Taklimakan and Australian deserts was 0.5, -0.2, -1.0 and -0.4 K, respectively. However, they could not locate a clear threshold to separate dust aerosol from cloud for dust originating from NW Africa, Libya or the Iranian desert. Consequently, the negative values may vary for a single geographical region or being dependent on the density of the dust plume.

B) Hao and Qu (2007) found that the brightness temperature difference between the MODIS 3.7μm and 9.7μm channels were sensitive to the presence of dust and developed the Thermal-Infrared Dust Index (TDI):

$$\boldsymbol{TDI = C_0 + C_1 \times BT_{3.7\mu m} + C_2 \times BT_{9.7\mu m} + C_3 \times BT_{11\mu m} + C_4 \times BT_{12\mu m}} \quad (2)$$

where C_0 is −7.937, C_1 is 0.1227, C_2 is 0.0260, C_3 is −0.7068 and C_4 is 0.5883

The coefficients C_0 to C_4 are determined through regression analysis between AOD and the brightness temperature measurements. Since the TDI uses just the thermal wavebands

it can operate both day and night (Chomette, Legrand and Marticorena 1999; Hansell et al. 2007). However, to date this index has only been validated over the oceans (Shahrisvand and Akhoondzadeh 2013).

C) Roskovensky and Liou (2005) developed the D-parameter algorithm to identify and separate cloud from atmospheric dust using differences in emissive and reflective wavelengths by combining the brightness temperature difference BTD (11μm - 12μm) with a reflectance ratio of the red (0.54 μm) and near infrared (0.86μm) wavebands:

$$\boldsymbol{D = \exp\{-\left[\frac{R_4}{R_{16}}a + \left(BT11_{\mu m} - BT12_{\mu m}\right) - b\right]\}} \quad (3)$$

where a is a scaling factor (a = 0.8) and b is a thermal offset (b = 2.0). Pixels where D > 1.0 are defined as being dust affected. Roskovensky and Liou (2005) found that inclusion of the reflectance ratio reduces the number of false detections over land and the false detection due to cirrus clouds that have similar reflectance and BTD properties to fine dust particles.

D) Qu et al. (2006) found that the reflectance of dust generally increases with wavelength between 0.4 and 2.5 μm whilst the cloud has the highest reflectance in MODIS band 3 (0.469 μm). Qu et al. (2006) developed the normalized difference dust index (NDDI) which exploits this characteristic :

$$\boldsymbol{NDDI = \frac{(R2.13_{\mu m} - R0.469_{\mu m})}{(R2.13_{\mu m} + R0.469_{\mu m})}} \quad (4)$$

NDDI values > 0.28 are defined as being dust affected and when applied to nine dust events over Gobi, the NDDI was found to be able to differentiate dust storms from water and ice clouds and some surface features. However, the approach was less successful over arid surfaces where the BT of MODIS band 31 (10.78–11.28 μm) was used to separate

atmospheric dust from surface sand (Qu et al. 2006). The NDDI has been successfully applied over both Asian and African regions (Han et al. 2013).

E) After analysing the efficiency of several of the most widely used algorithm's for detecting dust in Middle East region, Karimi et al. (2012) developed the Middle East Dust Index (MEDI). The MEDI uses MODIS band 29 (8.5μm) to enhance the difference between dust and desert surfaces. The MEDI is defined as:

$$\boldsymbol{MEDI} = \left[\frac{(\boldsymbol{BT11_{\mu m}} - \boldsymbol{BT8.5_{\mu m}})}{(\boldsymbol{BT12_{\mu m}} - \boldsymbol{BT8.5_{\mu m}})}\right] \quad (5)$$

Pixels with a value >0.6 were classified as being dust contaminated. Based on the visual comparison for the results of other methods, results of MEDI method implemented in the three storms studied show its capability to separate dust from desert surfaces (Karimi et al. 2012). For example, the main challenge of the Ackerman (1987) and Roskovensky and Liou (2005) methods was misclassifying desert surfaces as dust and this was greatly reduced by involving band 29 (8.5μm) in MEDI method. However, it is possible that this case is not constant where the assessment was carried out between the methods only in three dust events.

It is often difficult to inter-compare the performance of different algorithms as they are often used in different geographical regions or may use different instruments. To better comprehend the algorithm's performance relative to one another, they need to be applied to the same datasets over the same region. Thus, the performance of the algorithms was evaluated based on the seasonal variation of dust activity in the Middle East (early, peak and end season) at the same observational conditions. In addition, to assess how well each method works using the published thresholds, we assess whether different thresholds result in better dust detection based on comparison to the manually identified dust events.

To determine the most appropriate threshold to discriminate dust-contaminated pixels from others in this region, ~30,000 pixels for each feature types (dust, bright surfaces, dark surfaces, water, cloud) were identified using the MODIS land cover data, MODIS cloud mask

and visual interpretation of dust. Bright and dark surfaces are defined as deserts/plains and vegetation respectively. The threshold value for each algorithm is derived separately for each dust event based on the frequency distribution of algorithm values (Figure 2a). In each event, peaks were found to be attributable to specific features (e.g. dust, cloud and water bodies), and threshold values were adjusted to characterize the value which was best able to detect dust in the scene. For example, figure 2a illustrates the frequency distribution of BTD values (Ackreman 1997) derived for different surface types. Peaks representing dust (red line) are relatively easy to detect and separate it from other features (e.g. cloud and water) but a high percentage of pixels over bright and dark surfaces have similar BTD values (dust < 0.04) and would therefore be incorrectly identified as being dust contaminated (Figure 2b). Table 2 includes a summary of the published threshold values for each of the algorithms and the adjusted threshold values used to differentiate dust from non-dust in each of the dust events studied here. The published threshold values are very sensitive to several factors including dust mineralogy and density, surface reflectance and atmospheric conditions (Darmenov and Sokolik 2005), but they allow a certain degree of tuning to adjust for specific conditions such as regional variability or for dust blowing over land or ocean (Roskovensky and Liou 2005).

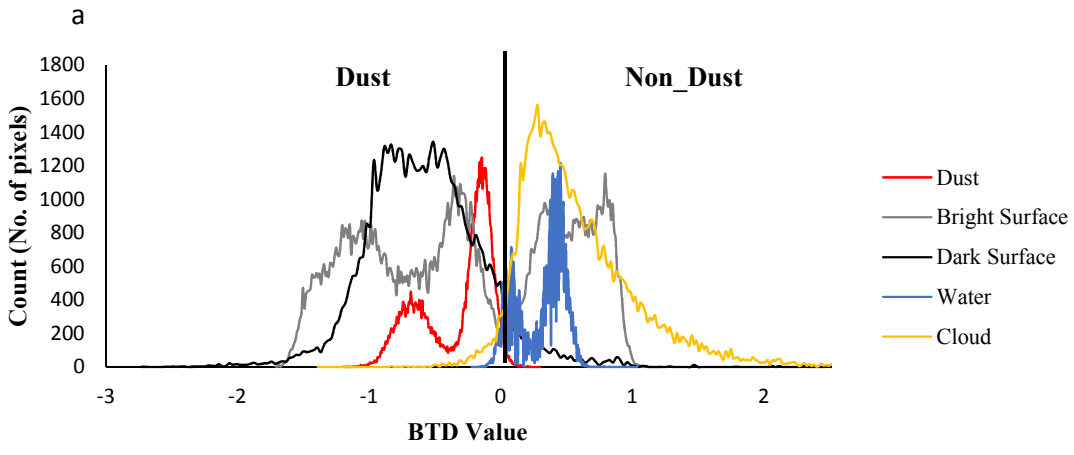

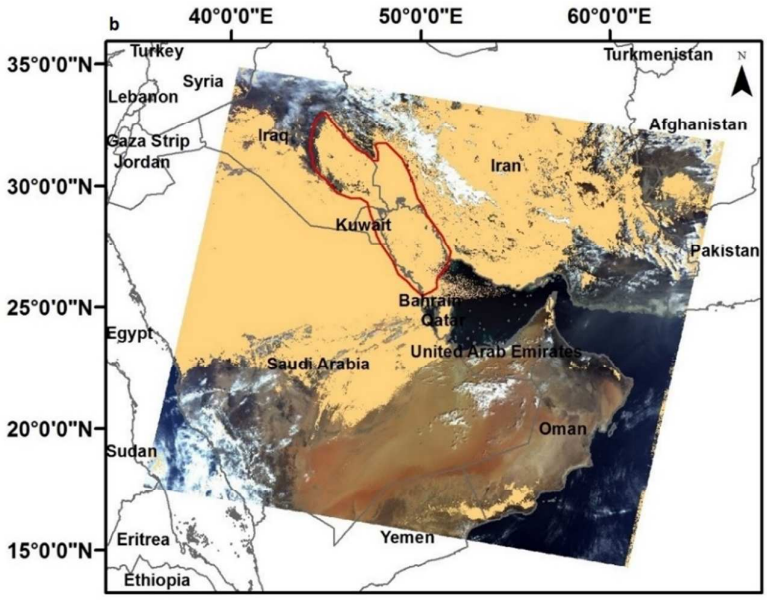

Figure 2. Histogram (a) illustrating for the variation in pixel BTD (Ackerman, 1997) values for different land surface types and for cloud and dust affected pixels from a single MODIS Terra image (b; Dust/non-dust threshold applied to BTD).

Table 2. Comparison of recommended dust/non dust thresholds and thresholds identified for events described in this study.

Algorithm	Published threshold values	dust/non-dust thresholds determined in this study					
		Event1		Event2		Event3	
		Terra	Aqua	Terra	Aqua	Terra	Aqua
Ackerman (1997) (BTD)	Dust < 0	Dust < 0.04	Dust < 0.26	Dust < -0.9	Dust < 0.87	Dust < -0.77	Dust < 0.4
Roskovensky and Liou (2005) (D-Parameter)	Dust > 1	Dust > 1.75	Dust > 0.72	Dust > 0.2	Dust > 0.16	Dust > 0.63	Dust > 0.2
Qu et al. (2006) (NDDI)	Dust > 0 or 0.28	Dust > -0.48	Dust > -0.54	Dust > -0.2	Dust > -0.25	Dust > 0	Dust > 0
Hao and Qu (2007) (TDI)	Dust > 1	Dust > 1.022	Dust > 1.1	Dust > 1	Dust > 0.6	Dust > 0.87	Dust > 1.25
Karimi et al. (2012) (MEDI)	Dust < 0.6	Dust < 1	Dust < 0.9	Dust < 1	Dust < 1.07	Dust < 1.4	Dust < 1.15

In this study, the basis for the comparison of the algorithms is the identification of dust events through visual inspection and aerosol optical depth (AOD) measurements from the MODIS data. The performance of the dust detection algorithms is assessed by

determining the omission and commission rates for each algorithm and comparing the percentage common pixels detected by all methods as dust-free and dust contaminated.

4. Validation with AERONET data

Although ground-based measurements from air quality monitoring networks provide information on atmospheric composition they are rarely available in near-real-time close to the main dust sources (Song et al. 2007). The majority of stations are located in urban or industrial areas, which are dominated by anthropogenic particles. In addition, the observational values are generally limited to the concentration of particulate matter (PM) with an aerodynamic diameter <10 μm (PM10), which does not always encompass the full size distribution of dust particles suspended in the atmosphere (Song et al. 2007). The Middle East region has no freely available air quality information data. However, with some assumptions, dust can be estimated from AERONET observations which enable the separation of fine and coarse mode aerosols (Dubovik et al. 2002; Basart et al. 2009; Kim et al. 2011). Basart et al. (2009) used AERONET observations to characterise atmospheric aerosols for regions including Middle East and found that dust at coastal stations, such as Abu Dhabi and Bahrain, had an AOD maxima of 1.5 and Ångström Exponent (AE) < 0.75. In contrast, they found that inland stations, such as Hamim and Solar Village, dust was associated with AOD ranging from 0.7 to 2 with AE < 0.75.

In this study we investigated dust characteristics over the Middle East between January to December 2015 using AERONET Level 2 data acquired at seven stations (Figure 1) and cloud screened following the method of Smirnov et al. (2000). The AERONET products used are AOD at 500nm, Ångström exponent (AE) and coarse mode and fine mode values at 500 nm. Observations with high Ångström exponent and fine mode fraction are discarded in order to restrict the estimation to conditions in which mineral dust is the dominant aerosol type. Parajuli, Yang and Lawrence (2016) suggested that the AERONET

AOD and coarse mode at 500 nm can be used to identify the dust with the value higher than 0.75 at Mezaira station. Similarly, Basart et al. (2009) found that dust is linked with high AOD ranging from 0.7 to 2 and with AE less than 0.75 at desert stations such as Hamim and Solar Village. For this reason, AERONET AOD at 500 nm >0.75 and which are accompanied by a low Ångström exponent and fine mode fraction are used to identify observations that are dust contaminated.

To validate the efficiency of dust detection methods in the Middle East, satellite dust detections over the AERONET sites were compared to the AERONET measurements. The AERONET measurements were collocated with dust detection algorithms applied to Terra and Aqua observations, both temporally and spatially. For AERONET measurements, valid values within ±15min of the MODIS overpass for each satellite were averaged. For each dust detection algorithm, pixel values at AERONET station site with a spatial resolution of 1km were selected. The agreement between AERONET data and algorithms as well as false detection are calculated by using following equations:

$$\text{Agreement} = \mathrm{D}_{Aer\&alg}/\mathrm{D}_{Aer}$$

$$\text{False detection} = 1 - \mathrm{D}_{Aer\&alg}/\mathrm{D}_{alg}$$

Where $\mathrm{D}_{Aer\&alg}$ denotes the number of dust events defined by both the dust detection algorithms and the AERONET observations, simultaneously. D_{Aer} and D_{alg} denote the number of dust events detected by the AERONET data and the dust detection algorithms, respectively.

5. Results

5.1. *Event1: The early season of dust activity*

A large dust event was identified over the Persian Gulf and along the Iran-Iraq on 5th February (2007) which was captured by both the Terra (07:20 UTC; Figure 3a) and Aqua

(10:30 UTC) satellites. The MODIS Terra visible image is shown in figure 3a where the red polygon indicates the extent of the dust storm that has been manually digitized. For reference, the MODIS AOD estimates (Figure 3b) and MODIS cloud mask (Figure 3c) are shown where the latter correctly detects cloud affected pixels (black) but not dust contaminated pixels. However, during heavy atmospheric dust concentrations the MODIS cloud mask product may flag the dust-laden atmosphere as cloud (Ackerman et al., 1998).

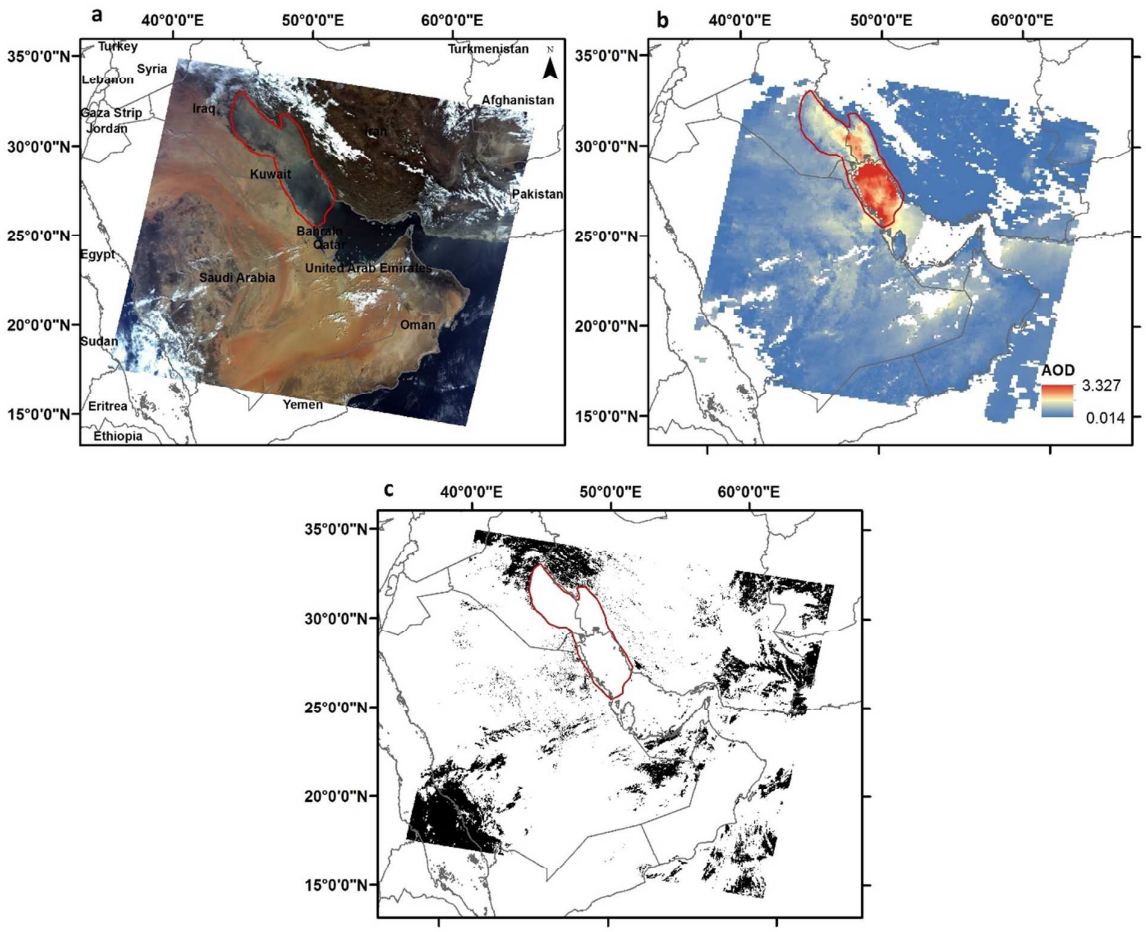

Figure 3. Spatial variability of the dust storm on 5th February 2007 (Terra) outlined by the red polygon: (a) MODIS true colour composite (bands 1, 4 and 3); (b) MODIS AOD image and (c) MODIS cloud cover mask.

These polygons (red colors) were compared with MODIS AOD measurements as no in-situ dust concentration data were available for the period for which the dust storm was detected. Using MODIS AOD observations, groups of pixels (~2000 pixels) were extracted that occurred in dust-affected and clear sky regions. Figure 4 illustrates that distinct differences in AOD magnitude are evident between clear sky land and water whilst dust contaminated land and water differ by on average 0.52 but share a degree of overlap.

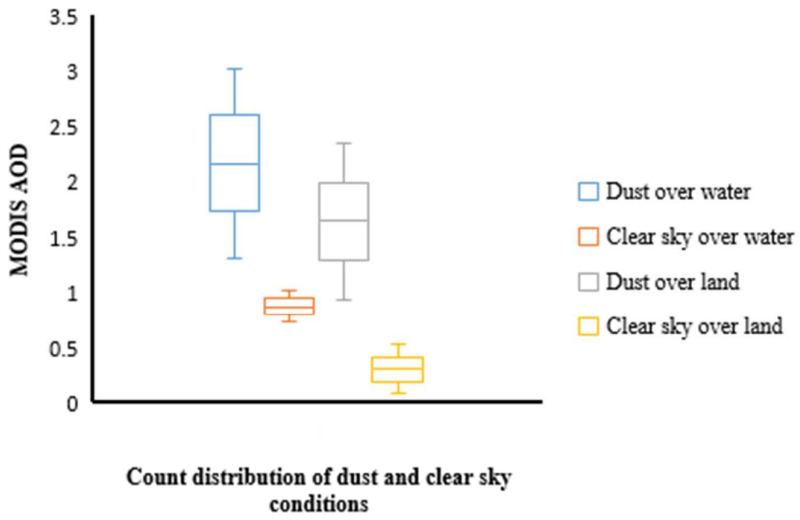

Figure 4. Mean MODIS AOD distribution of dust affected water and clear-sky water and dust affected land and clear sky land. The boxes define the values of MODIS AOD for dust-affected land and water and clear-sky land and water with medians; whiskers represent the range of the AOD values found in these cover types.

Figures (5a-e) illustrates the spatial distribution of detected dust contaminated pixels for each of the five algorithms. The spatial agreement between the MODIS satellite AOD product (Figure 3b) and dust detection methods is good within the dust polygon. Under heaviest dust concentrations (AOD > 1) all methods are typically able to detect dust contaminated pixels with detection rates of between 90.7 and 97.4% for the Terra image (Table 3). However, over dust free regions, which are characterized by lower MODIS AOD

values, a significant proportion of the MODIS image is identified as being dust contaminated, particularly over land. Similar results are found with the afternoon Aqua image (not shown). It is clear that considerable variations exist between and within the performances of the various techniques across the range of the tested images. The percentage of the non-dust affected image detected as being dust contaminated are 89.6 and 90.5% (BTD), 88.9 and 90.6% (D-parameter), 94.4 and 95.2% (NDDI), 94.3 and 95.1% (TDI) and 90.7 and 92.7% (MEDI) for both Terra and Aqua images. The NDDI (Figure 5c) and TDI (Figure 5d) have the highest commission rates perform whilst the BTD (Figure 5a) and D-Parameter (Figure 5b) perform slightly better and typically separate dust and cloud contaminated pixels. The MEDI algorithm (Figure 5e), which was developed for application over this region, performs on a similar level as the BTD and D-parameter algorithms and incurs a large percentage of false detections over desert.

In general, the results indicate that the adjusted thresholds (Table 2) for all methods were suitable for detecting a high proportion of the dust-affected pixels but this comes at the expense of significant false alarm rates over the land surface.

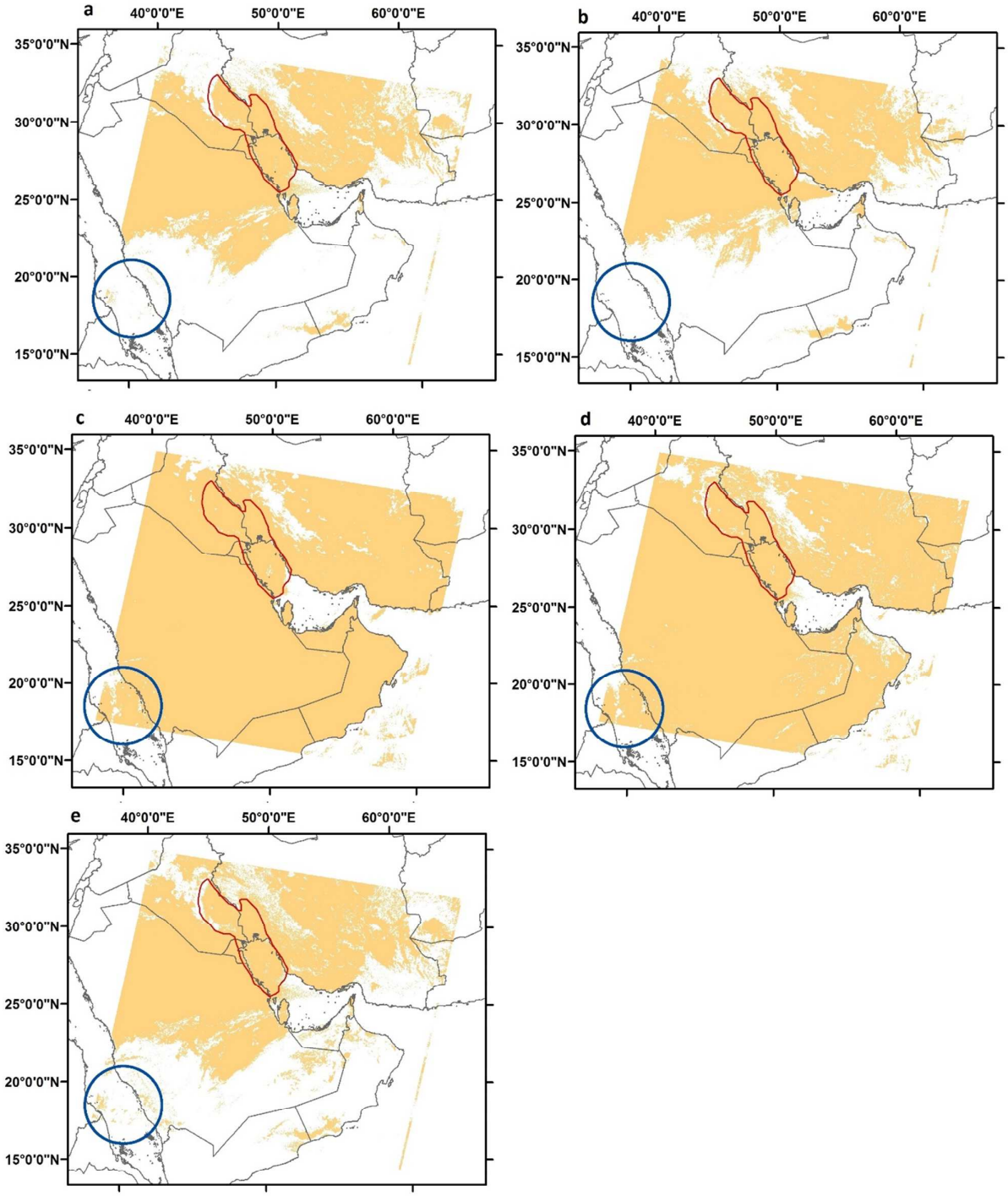

Figure 5. Spatial variability of the dust detection methods results on 5th February 2007 (Terra): (a) Ackerman (1997) (BTD); (b) Roskovensky and Liou (2005) (D-Parameter); (c) Qu et al. (2006) (NDDI); (d) Hao and Qu (2007) (TDI) and (e) Karimi et al. (2012) (MEDI).

The blue circle indicates regions of cloud that have been incorrectly identified as dust. The adjusted dust/non-dust thresholds used for event 1 are detailed in table 2.

Table 3. Percentages (%) of identified dusty pixels relative to the reference data (manually dust detection) and the commission and omission errors for early season event.

Methods	Terra			Aqua		
	Dust Detection (%)	Commission	Omission	Dust Detection (%)	Commission	Omission
BTD	90.76	89.62	9.24	97.54	90.58	2.46
D-parameter	94.72	88.99	5.28	95.82	90.61	4.18
NDDI	97.47	94.42	2.53	97.63	95.24	2.37
TDI	96.72	94.31	3.28	96.64	95.19	3.36
MEDI	90.73	90.76	9.27	93.89	92.7	6.11

5.2. *Event 2: The peak season of dust activity*

On 26th June, 2007, a trail of dust originated from Syria and moved towards Iraq, Saudi Arabia, and the northern region of the Persian Gulf and MODIS Terra captured the dust storm. The dust plume AOD concentrations ranged between 1.1 and 4.3 (average AOD of 2.7) but despite having a high average AOD the dust detection algorithms again perform weakly with only the D-Parameter algorithm detecting over 99.9% of the dust contaminated pixels (Table 4). The remaining algorithms tended to detect dust contaminated pixels over the land surface but detect a lower proportion of those over water. This is due to the spectral signature of dust not being distinctly different from the water surface in the bands used by these methods. Variation in the detection rates between Terra and Aqua may also result from the difference in view zenith angles (and path length) that the event was observed where the former had an average view zenith angle of 55° whilst Aqua had an average view zenith angle of 10°. All of the algorithms contain significant false alarm rates that range between 73.0% (BTD) and 97.7% (MEDI) as shown in table 4. Large commission errors are also evident in the MODIS Aqua scene although the performance of the algorithms is somewhat

different. A number of the algorithms (BTD, D-Parameter and NDDI) effectively discriminated between cloud and dust but the D-Parameter and NDDI perform most favourably although with high commission rates. The inclusion of optical wavebands in addition to the BTD provides better separation between dust and clouds due to the differences in scattering and absorption at visible wavelengths (Qu et al. 2006).

Table 4. Percentages (%) of identified dusty pixels relative to the reference data (manually dust detection) and the commission and omission errors for peak season event.

Methods	Terra			Aqua		
	Dust Detection (%)	Commission	Omission	Dust Detection (%)	Commission	Omission
BTD	55.04	73.06	44.96	98.73	73.86	1.27
D-parameter	99.95	89.66	0.05	99.6	76.84	0.4
NDDI	82.67	93.96	17.33	98.46	83.6	1.54
TDI	87.9	97.09	12.1	99.4	83.13	0.6
MEDI	65.37	97.73	34.63	33.37	82.44	66.63

5.3. *Event 3: The end season of dust activity*

Despite being the season with the lowest frequency of dust events (Kutiel and Furman, 2003), large dust events occur in September as a result of the 'winter Shamal' which provides some of the strongest winds of the season over the Persian Gulf. On 12th September (2007) a dust storm originating in Saudi Arabia blew across the Persian Gulf, Qatar, and Bahrain.

All of the dust algorithms detect the plume on both images over land although the distribution of dust detections there was little spatial correspondence with the spatial variation of MODIS AOD. Table 5 indicates the omission and commission rates of each algorithm for each MODIS image. It is evident that the best performing algorithm is D-Parameter but that all algorithms perform poorly in either the Terra or Aqua imagery. By adopting the adjusted thresholds of D-parameter method, it correctly identifies >98% of the dust contaminated pixels but it also has the highest commission error.

Table 5. Percentages (%) of identified dusty pixels relative to the reference data (manually dust detection) and the commission and omission errors for end season event.

Methods	Terra			Aqua		
	Dust Detection (%)	Commission	Omission	Dust Detection (%)	Commission	Omission
BTD	54.7	81.39	45.3	91.33	92.03	8.67
D-parameter	98.62	94.34	1.38	99.25	94.96	0.75
NDDI	64.87	96.09	35.13	62.3	96.71	37.7
TDI	76.56	94.93	23.44	85.54	96.04	14.46
MEDI	48.29	86.54	51.71	96.39	95.39	3.61

In general, all algorithms provide a simple means to detect dust contaminated pixels with an average detection rate (between all algorithms) of 85%. Among the dust events assessed here, the D-parameter algorithm is the only method that has a satisfactory omission rate (0-5%). On the other hand, all algorithms have extremely high commission errors for all events. The changing in their performance may results from variations in dust altitude and thickness (Herman et al. 1997) or changes of dust mineral composition and size (Torres et al. 1998).

Table 6 shows these events as percentage of shared pixels with respect to the total number of pixels found in the dust plume region (identified by the red polygons). The results indicate that there are considerable differences in the percentage to which the all algorithms agree for pixels containing dust that range between 33% and 90.1% within the dust plume regions. This demonstrates that there is significant variability in the performance of some algorithms among the dust events. One possibility is that some algorithms are actually more sensitive to variations in dust mineralogy than others, in particular MEDI method. It can be noted that the shared pixels of the non-dust (omission error) is close to zero for all provided images, which illustrates that the manual dust detection procedure effectively and accurately

identified dust contaminated pixels, where as a minimum one method concur with these polygons. The table also shows the percentage of shared pixels (commission error) in relation to the total number of pixels in the original images excluding the total pixels within the red polygons. The commission error is high in some images indicating that all of the dust algorithms may share the same error (explored in section 5.4).

Table 6. Percentages agreement (%) of identified dusty pixels relative to the reference data (manually dust detection) and the commission and omission errors for all events.

Agreements between all methods	Event1: Early season		Event2: Peak season		Event3: End season	
	Terra	Aqua	Terra	Aqua	Terra	Aqua
Shared pixels (dust)	87.95	90.12	54.78	33.06	44.45	61.67
Shared pixels (Omission)	0.50	0.36	0.00	0.00	0.06	0.03
Shared pixels (Commission)	39.81	37.77	4.13	0.35	7.95	24.91

5.4. *Evaluation of dust detection algorithms with respect to the cloud cover and background*

The results from the previous section indicate that cloud cover and the surface characteristics can have a significant impact on the utility of each index for dust plume detection. Here we test the capability of each dust index to differentiate dust-contaminated and uncontaminated pixels using the MODIS land cover map and MODIS cloud mask. A region of interest, containing >30,000 pixels for each feature (clouds, water, dark & bright surfaces), was manually selected to assess number of false detections which are given in table 7. It is apparent that the TDI and NDDI algorithms perform better over water than over the land but that their ability to distinguish between cloud and dust is quite variable. Amongst all these methods, the TDI has the highest false detection of dust with respect to cloud cover. By obtaining the highest dust detection rate and being the best at separating dust from cloud, the

D-Parameter is the worst performing over other surfaces such as water, dark & bright surfaces.

The MEDI algorithm has difficulty discriminating dust from both dark surfaces and desert areas where it performed effectively in some cases, yet was ineffective in others. Using this algorithm, Moridnejad et al. (2015) demonstrated good agreement with results obtained by Ginoux et al. (2012) in terms of dust source identification. Similarly, BTD has been proven to be a reliable method for the identification of dust sources (Baddock et al. 2009; Karimi et al. 2012). However, two faults evident from table 7 concerning the BTD algorithm are that it misclassifies bright land (mainly the desert surfaces) as dust plumes and provides inconsistent separation of dust affected regions from dark surfaces or cloud covered regions. Therefore, this method is best suited to the detection of dust over water bodies. Vegetation cover, which is predominantly grasslands and semi-desert shrubs, has a phenological cycle which will alter the surface emissivity and reflectivity and, thus, in the performance of the methods. Using the red and near infrared wavebands bands of the images, the mean (standard deviation) of the Normalized Difference Vegetation Index (NDVI) for the vegetated areas is 0.27 (0.10), 0.19 (0.05) and 0.17 (0.04) for event 1, event 2 and event 3, respectively which suggests these are sparsely vegetated surfaces. However, the results indicate that all methods perform poorly over dark surfaces for all events with average false alarm rates of 97.7% (event1), 58.7% (event2) and 74.5% (event3). It was also found that the MEDI algorithm can be sensitive to the emissivity variability of vegetated surfaces where the false alarm rate ranges from 0.2% to 99.6%. On the other hand, the false detection rates for all methods may improve over the high densely vegetated surfaces because of the high contrast of some bands used (e.g. BTD) between the dust and these surfaces.

Table 7. Percentages (%) of misidentified dust contaminated pixels by dust detection algorithms relative to different image features. (False detection).

background	BTD method					
	Event1:Early Season		Event2: Peak Season		Event3: End Season	
	Terra	Aqua	Terra	Aqua	Terra	Aqua
bright	60.49	52.68	57.30	100.00	0.00	91.17
Dark	93.29	99.48	NULL	32.05	NULL	30.44
Water	1.30	0.00	0.00	2.39	0.00	1.36
Cloud	4.20	64.22	0.00	43.33	0.00	84.43

background	D-Parameter method					
	Event1:Early Season		Event2: Peak Season		Event3: End Season	
	Terra	Aqua	Terra	Aqua	Terra	Aqua
bright	51.37	44.05	98.87	100.00	29.34	95.58
Dark	97.17	99.58	NULL	90.84	NULL	94.48
Water	11.80	3.17	97.83	80.83	76.98	99.99
Cloud	0.30	0.00	0.03	0.12	0.08	0.00

background	NDDI method					
	Event1:Early Season		Event2: Peak Season		Event3: End Season	
	Terra	Aqua	Terra	Aqua	Terra	Aqua
bright	100.00	100.00	100.00	100.00	99.99	100.00
Dark	99.52	100.00	NULL	99.11	NULL	61.00
Water	0.28	0.56	0.00	0.00	0.00	0.00
Cloud	77.19	78.08	0.00	3.25	0.00	0.15

background	TDI method					
	Event1:Early Season		Event2: Peak Season		Event3: End Season	
	Terra	Aqua	Terra	Aqua	Terra	Aqua
bright	100.00	100.00	100.00	100.00	58.61	100.00
Dark	94.86	100.00	NULL	71.44	NULL	96.75
Water	0.43	0.03	0.03	0.02	0.01	0.04

Cloud	94.21	99.14	99.67	96.56	99.98	99.85
background	**MEDI method**					
	Event1:Early Season		**Event2: Peak Season**		**Event3: End Season**	
	Terra	**Aqua**	**Terra**	**Aqua**	**Terra**	**Aqua**
bright	62.03	72.66	82.76	0.00	0.00	100.00
Dark	93.41	99.67	NULL	0.23	NULL	89.87
Water	8.20	0.82	15.56	2.39	0.00	44.28
Cloud	28.20	50.82	96.17	27.02	0.23	87.76

5.5. *A comparison of seasonal MODIS-derived dust detections against AERONET measurements*

As evident from previous sections, the identification of dust is complex and there are no instruments that can provide direct measurements of dust with which to validate satellite products. Figure 6 presents an example of daily dust detections over inland Sede Boker site as indicated by each of the dust algorithms. It indicates that, based on the threshold applied here, AERONET detects 8 days as being dust contaminated. In contrast, the EO dust algorithms detect between 4 and 7 days as having been dust contaminated. There is little correspondence between the satellite detections from any algorithm and the peaks and troughs of AERONET AOD.

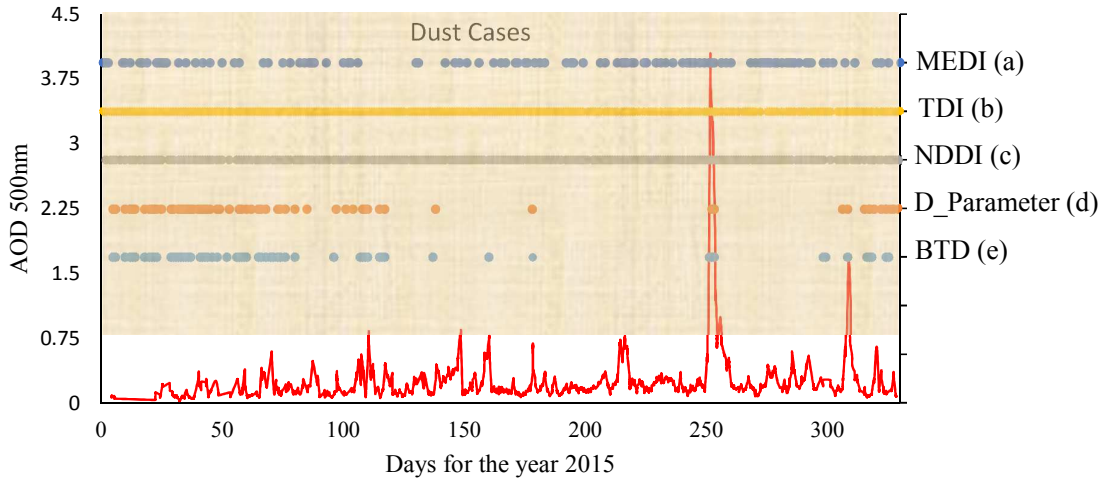

Figure 6. The long-term daily AOD 500nm at Sede Boker (red) site and dust cases results by each algorithm for the daily data of Terra and Aqua. The dusty days detected by AERONET (algorithms) are 110 (b, c, d, e), 148 (a, b, c), 251 (a, b, c, e), 252 (all), 253 (all), 255 (c), 308 (b, c, d, e) and 309 (b).

Table 8. Summary of the comparison between dust cases between dust detection methods and AERONET data.

Name	Available data range (2015)	No. of Dust events (AERONET Stations)	Agreement (false detection)				
			BTD	D-parameter	NDDI	TDI	MEDI
Eilat	Jan_Dec	7	0.571 (0.953)	0.857 (0.973)	1.000 (0.974)	0.714 (0.986)	0.429 (0.977)
KAUST Campus	Apr_Aug	33	0.424 (0.417)	0.576 (0.648)	0.667 (0.835)	0.970 (0.816)	0.242 (0.778)
Masdar Institute	Mar_Dec	26	0.231 (0.778)	0.154 (0.886)	1.000 (0.937)	1.000 (0.933)	0.308 (0.929)
Mezaira	Mar_Dec	26	0.308 (0.875)	0.269 (0.889)	0.962 (0.952)	0.923 (0.947)	0.115 (0.917)
SEDE BOKER	Jan_Nov	8	0.625 (0.943)	0.500 (0.952)	0.875 (0.987)	0.875 (0.986)	0.500 (0.970)
Shagaya Park	Aug_Dec	8	0.500	0.500	1.000	0.750	0.250

			(0.946)	(0.945)	(0.964)	(0.975)	(0.909)
Weizmann Institute	Jul_Nov	8	0.250 (0.778)	0.375 (0.786)	0.500 (0.967)	0.750 (0.914)	0.625 (0.959)

The results indicate that a varying level of agreement between the AERONET dust detections at all sites and those from the EO dust detection algorithms (Table 8). Overall, the NDDI provided the greatest agreement with AERONET and detects, on average, 85.7% of the AERONET detections. However, it also has the highest false alarm rate with an average of 94.5%. The BTD and D-parameter algorithms typically have the least agreement with AEORNET but also the lowest (albeit high) false alarm rate. For all AERONET stations, the dust detection methods overestimate dust cases. The large inconsistency between the methods and AERONET measurements of the observed dust during a large part of the year and at different locations suggests these methods are influenced by aerosol types other than dust from marine and anthropogenic sources. This influence is evident as shown in figures 7 (a-b), where the high Ångström exponent and fine mode fraction values indicate the presence of small non-dust particles that were estimated over Eilat site on January 14 (2015). These non-dust particles have incorrectly detected as dust using all of the dust algorithms.

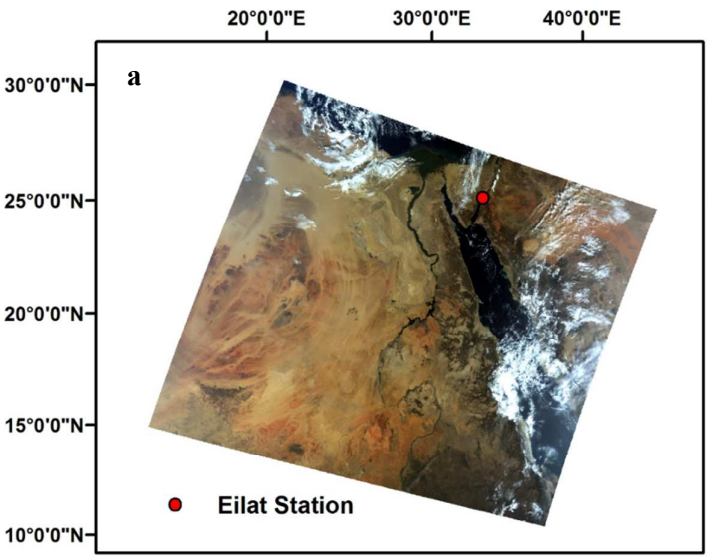

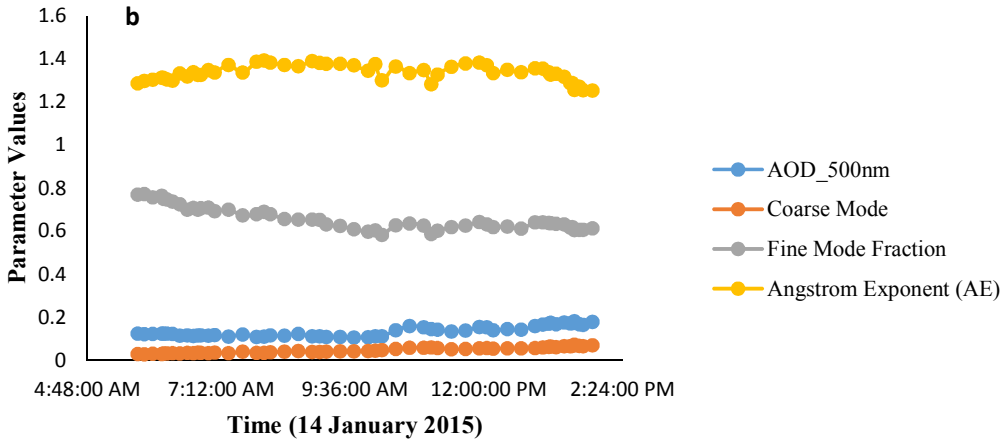

Figure 7. Non-dust case on 14 January 2015. (a) MODIS true colour composite (bands 1, 4 and 3) and location of AERONET Eilat station. (b) the observations of AOD and its associated parameters at 500nm at Eilat station.

6. Discussion

Three different dust events were assessed in this study, where dust plume in event 1 (early season) was observed originating from the alluvial plains of Iraq which may dominated by silt and clay (Warner 2009), dust event 2 (peak season) originated from Syria which may dominated by clay (Anderson 2004) and the origin of the event 3 (end season) was from the Rub Al Khali desert which is dominated by fine sands (Abdelfattah 2009). For all events, we can confirm that all the dust detection methods used here make it easier to detect dust with an average detection rate of 85% between all algorithms. The results commonly place D-parameter in one group (as the best), then followed by BTD, TDI and NDDI in succeeding group, whilst the MEDI method remains alone in another group (the worst). However, all of the algorithms contain significant false alarm rates that range between 73.06% (BTD- the lowest) and 97.73% (MEDI- the highest) for all events.

Results indicate that the adjusted threshold for D-Parameter algorithm worked effectively for all events, at least for highlighting dust plumes but large areas of land surface were also included. For all events, the D-Parameter algorithm detected over 90% of the dust

contaminated pixels and it clearly differentiated cloud from the main dust plumes. In contrast, this algorithm is the worst performing over water. The results indicate that all dust detection methods perform ineffectively over bright and dark surfaces for all events with an average false alarm rate of 75% and 82% over bright and dark surfaces, respectively. A similar trend was evident in all dust detection algorithms which is supported by Jafari and Malekian (2015) who also noted the poor performance of the dust detection algorithms which included the BTD (Ackerman 1997), Miller (2003), D-parameter (Roskovensky and Liou 2005), NDDI (Qu et al. 2006) and TDI (Hao and Qu 2007) differed from two dust events that were originated from Iraq and Saudi Arabia. The Ackerman (1997) and Roskovensky and Liou (2005) algorithms were applied to four significant dust events from the Lake Eyre Basin, Australia, that were originated from the dune sands (which are iron-rich) and from the bed of Lake Eyre (which are illite-rich) (Baddock, Bullard, and Bryant 2009). Baddock, Bullard, and Bryant (2009) found that both algorithms were successful in detecting dust, but their effectiveness in dust source determination varied from event to event. This suggests that the poor performance of the dust detection algorithms is not associated to specific dust sources. Given that the spectral properties of dust are influenced by dust mineralogy amongst other factors, a greater number of dust events from different regions should be evaluated so that the impact of these issues can be quantified.

It is evident that the efficiency of dust detection methods varied across locations. Based on visual interpretation for all events, the results found that BTD and D-parameter methods were perform poorly in differentiate dust from non-dust in Saudi Arabia whereas they were perform effectively over land surface in UAE and Oman. Hence, the disparities in soil characteristics and types could largely affect the performance of the methods on over land. Consequently, a number of factors like water composition, chemical contents, shape, roughness as well as wavelength, and view zenith angle are attributed to have a role in the

process and may be the point of concern in subsequent investigations (El-Askary et al. 2003; Satheesh and Moorthy 2005). Among the prevalence errors is the inability of the algorithms to differentiate between dust and other features in the image. In arid and semi-arid lands, the dust detection algorithms fail to distinguish dust from bright lands which is noted in other studies (Kaufman et al. 2002; Baddock, Bullard, and Bryant 2009) but which limits their application to address social and environmental concerns. This study identified that it was possible to reduce the prevalence of commission errors by raising the threshold and consequently increasing the omission errors, and vice versa. Despite this, the commission and omission error rates remain unacceptable for all the events studied.

However, no algorithm assessed in this study is applicable to all scenarios. The Roskovenesky and Liou (2005) method was developed to differentiate dust from clouds whilst the Ackerman (1997) algorithm demonstrated that BTD between 11 and 12nm was useful in detecting dust over an ocean. The results here support this and indicate the two methods can reach their goal over the Middle East with average false alarm rates of 0.8% (for separating dust from water using BTD algorithm) and 0.08% (for separating dust from cloud using D-parameter method). However, the methods also have disadvantages such as their failure to distinguish dust from other features such as bright and dark surfaces that are important in the detection of dust using EO data. Despite the challenges faced in differentiating dust and bright and dark surfaces, all algorithms, with the exclusion of D-parameter algorithm, were able to separate dust from water. Comparison of the daily temporal detection rate of the dust algorithms against daily AERONET detected dust indicates significant discrepancies between dust events derived by the algorithms and AERONET data. Although the EO methods were successfully detecting some dust events with high AERONET AOD values, they typically had very high false detection rates even on days where AERONET AOD values were low. The high false detection rate is due in part to

not only the sensitivity to non-dust aerosols but also by the uncertainties in resolving the surface properties.

Identification of dust sources and the regions covered by the movements of particles and their impact have the highest propriety for scientist and policy makers. Despite the advantages offered by dust detection algorithms, the effective detection of airborne dust still represents a challenge for researchers. One of the key challenges is the detection of airborne dust over bright surfaces (e.g., desert regions) because of the larger contribution of these surfaces to the radiance received by satellite sensors. The results of this study indicate that the visible and near-infrared (VIR)-based approaches have difficulty detecting dust over their originating regions (i.e., desert, arid and semiarid regions), restricting their application to over water such as oceans. It is likely that these approaches are extremely sensitive to high albedo surfaces. In contrast, the thermal-based approaches have shown better efficiency, but not fully success, in detecting dust storms over bright land surfaces. The common notion among the thermal-based approaches is that dust pixels have significantly different values of BTD than non-dust background. However, there are several factors that may affect the performance of this approach including, atmospheric effects, surface emissivity, solar/sensor viewing geometries; and non-uniform dust scenes. Future development of dust detection algorithm should consider evaluating the performance of the algorithm under a wide range of atmospheric, viewing and surface condition to ensure applicability at global scale.

7. Conclusions

Earth Observation data provides a unique opportunity for studying the process of dust events at large scales, and in the areas with no ground measurements. This study evaluated the five commonly used dust detection algorithms applied to MODIS data to characterize the effectiveness of these algorithms to detect dust extent across the Middle East. The outcomes of dust detection with these algorithms are far from consistent in terms of numbers of dust

pixels detected, but agree reasonably well in terms of the spatial distribution of dust. The variation in these algorithms performance depended on the nature of spectral channels used and on the surfaces and features upon which the dust events occur. The majority of dust detection algorithms are reasonably efficient in removing false alarms by clouds (only D-parameter) and water surfaces, but none of the algorithms is capable of eliminating false alarms caused by bright or dark surfaces. There remains several issues for threshold-based dust detection methods as the published threshold values of these algorithms have to be significantly adjusted on an event-by-event basis. This may leads to limit their effectiveness for global or longer-term studies. It should also be noted that, to date, validation of dust detection algorithms remains a challenge. It is also important to stress that the results from this study may not be generalized because they are for a specific ecological and geographical domain.

Acknowledgements

The authors are grateful to the anonymous reviewers for their comments and suggestions that have helped to improve the manuscript. Authors gratefully acknowledge the NASA Land Processes Distributed Active Archive Center (LP DAAC) (https://lpdaac.usgs.gov/data_access) for providing free access to the MODIS data. We would also like to show our gratitude to AErosol RObotic NETwork (AERONET) site managers for provision of the AERONET data. We gratefully thank King Abdulaziz City for Science and Technology (KACST) for funding a studentship (Abdullah bin Abdulwahed).

References

Abdelfattah, M. A. 2009. "Land Degradation Indicators and Management Options in the Desert Environment of Abu Dhabi, United Arab Emirates." *Soil Horizons* 50 (1):3. doi: 10.2136/sh2009.1.0003.

Abdullah, M. A., and M. A. Al-Mazroui. 1998. "Climatological study of the southwestern region of Saudi Arabia. I. Rainfall analysis." *Climate Research* 9:213–23. doi: 10.3354/cr009213.

Ackerman, S. A. 1997. "Remote sensing aerosols using satellite infrared observations." *Journal of Geophysical Research: Atmospheres* 102 (D14):17069–79. doi: 10.1029/96jd03066.

Ackerman, S. A., K. I. Strabala, W. P. Menzel, R. A. Frey, C. C. Moeller, and L. E. Gumley. 1998. "Discriminating clear sky from clouds with MODIS." *Journal of Geophysical Research: Atmospheres* 103 (D24):32141-57.

Arimoto, R. 2001. "Eolian dust and climate: relationships to sources, tropospheric chemistry, transport and deposition." *Earth Science Reviews* 54 (1-3):29–42. doi: 10.1016/s0012-8252(01)00040-x.

Baddock, M. C., J. E. Bullard, and R. G. Bryant. 2009. "Dust source identification using MODIS: A comparison of techniques applied to the Lake Eyre Basin, Australia." *Remote Sensing of Environment* 113 (7):1511–28. doi: 10.1016/j.rse.2009.03.002.

Barkan, J., and P. Alpert. 2010. "Synoptic analysis of a rare event of Saharan dust reaching the Arctic region." *Weather* 65 (8):208–11. doi: 10.1002/wea.503.

Basart, S., C. Pérez, E. CUEVAS, J. M. Baldasano, and G. P. Gobbi. 2009. "Aerosol characterization in Northern Africa, Northeastern Atlantic, Mediterranean Basin and Middle East from direct-sun AERONET observations." *Atmospheric Chemistry and Physics Discussions* 9 (2):7707–45. doi: 10.5194/acpd-9-7707-2009.

Ben-Ami, Y., I. Koren, Y. Rudich, P. Artaxo, S. T. Martin, and M. O. Andreae. 2010. "Transport of Saharan dust from the Bodélé Depression to the Amazon Basin: a case study." *Atmospheric Chemistry and Physics Discussions* 10 (2):4345–72. doi: 10.5194/acpd-10-4345-2010.

Benedetti, A., J. M. Baldasano, S. Basart, F. Benincasa, O. Boucher, M. E Brooks, J. Chen, P. R. Colarco, S. Gong, and N. Huneeus. 2014. "Operational dust prediction." In *Mineral Dust*, 223-65. Springer.

Bener, A., Y. Abdulrazzaq, J. Al-Mutawwa, and P. Debuse. 1996. "Genetic and environmental factors associated with asthma." *Human biology*:405-14.

Berk, A. G. P. A., G. P. Anderson, P. K. Acharya, J. H. Chetwynd, L. S. Bernstein, E. P. Shettle, M. W. Matthew, and S. M. Adler-Golden. 1999. "MODTRAN4 user's manual." *Air Force Research Laboratory, Hanscom AFB, MA* 1731:3010.

Böer, B. 1997. "An introduction to the climate of the United Arab Emirates." *Journal of Arid Environments* 35 (1):3–16. doi: 10.1006/jare.1996.0162.

Brunekreef, B., and B. Forsberg. 2005. "Epidemiological evidence of effects of coarse airborne particles on health." *The European respiratory journal* 26 (2):309–18. doi: 10.1183/09031936.05.00001805.

Cakmur, R. V., R. L. Miller, and I. Tegen. 2001. "A comparison of seasonal and interannual variability of soil dust aerosols over the Atlantic Ocean as inferred by the TOMS AI and AVHRR AOT retrievals." *Journal of Geophysical Research: Atmospheres* 106 (D16):18287–303. doi: 10.1029/2000jd900525.

Caquineau, S., A. Gaudichet, L. Gomes, and M. Legrand. 2002. "Mineralogy of Saharan dust transported over northwestern tropical Atlantic Ocean in relation to source regions." *Journal of Geophysical Research: Atmospheres* 107 (D15).

Chomette, O., M. Legrand, and B. Marticorena. 1999. "Determination of the wind speed threshold for the emission of desert dust using satellite remote sensing in the thermal infrared." *Journal of Geophysical Research: Atmospheres* 104 (D24):31207–15. doi: 10.1029/1999jd900756.

Chu, P. C., Y. Chen, S. Lu, Z. Li, and Y. Lu. 2008. "Particulate air pollution in Lanzhou China." *Environment International* 34 (5):698–713. doi: 10.1016/j.envint.2007.12.013.

Chung, Y., H. Kim, J. Dulam, and J. Harris. 2003. "On heavy dustfall observed with explosive sandstorms in Chongwon-Chongju, Korea in 2002." *Atmospheric Environment* 37 (24):3425–33. doi: 10.1016/s1352-2310(03)00360-1.

Crooks, G. A., and G. R. C. Cowan. 1993. "Dust storm, South Australia, November 7th, 1988." *Australian Meteorological and Oceanographic Society* (77:693–720).

Darmenov, A., and I. N. Sokolik. 2005. "Identifying the regional thermal□IR radiative signature of mineral dust with MODIS." *Geophysical Research Letters* 32 (16).

Darmenova, K., I. N. Sokolik, and A. Darmenov. 2005. "Characterization of east Asian dust outbreaks in the spring of 2001 using ground□based and satellite data." *Journal of Geophysical Research: Atmospheres* 110 (D2).

Dubovik, O., B. Holben, T. F. Eck, A. Smirnov, Y. J. Kaufman, M. D. King, D. Tanré, and I. Slutsker. 2002. "Variability of Absorption and Optical Properties of Key Aerosol Types Observed in Worldwide Locations." *Journal of the Atmospheric Sciences* 59 (3):590–608. doi: 10.1175/1520-0469(2002)059<0590:voaaop>2.0.co;2.

Dubovik, O., and M. D. King. 2000. "A flexible inversion algorithm for retrieval of aerosol optical properties from Sun and sky radiance measurements." *Journal of Geophysical Research: Atmospheres* 105 (D16):20673–96. doi: 10.1029/2000jd900282.

El-Askary, H., R. Gautam, R. P. Singh, and M. Kafatos. 2006. "Dust storms detection over the Indo-Gangetic basin using multi sensor data." *Advances in Space Research* 37 (4):728–33. doi: 10.1016/j.asr.2005.03.134.

El-Askary, H. M., S. Sarkar, M. Kafatos, and T. A El-Ghazawi. 2003. "A multisensor approach to dust storm monitoring over the Nile Delta." *IEEE Transactions on Geoscience and Remote Sensing* 41 (10):2386-91.

Fischer, E. V., N. C. Hsu, D. A. Jaffe, M. J. Jeong, and S. L. Gong. 2009. "A decade of dust: Asian dust and springtime aerosol load in the U.S. Pacific Northwest." *Geophysical Research Letters* 36 (3):n/a-n/a. doi: 10.1029/2008gl036467.

Friedl, M. A., D. Sulla-Menashe, B. Tan, A. Schneider, N. Ramankutty, A. Sibley, and X. Huang. 2010. "MODIS Collection 5 global land cover: Algorithm refinements and characterization of new datasets." *Remote Sensing of Environment* 114 (1):168–82. doi: 10.1016/j.rse.2009.08.016.

Ginoux, P., J. Prospero, O. Torres, and M. Chin. 2004. "Long-term simulation of global dust distribution with the GOCART model: Correlation with North Atlantic Oscillation." *Environmental Modelling & Software* 19 (2):113–28. doi: 10.1016/s1364-8152(03)00114-2.

Ginoux, P., J. M. Prospero, T. E. Gill, N. C. Hsu, and M. Zhao. 2012. "Global-scale attribution of anthropogenic and natural dust sources and their emission rates based on MODIS Deep Blue aerosol products." *Reviews of Geophysics* 50 (3). doi: 10.1029/2012rg000388.

Goudie, A. 2013. *Arid and semi-arid geomorphology*. Cambridge: Cambridge University Press.

Goudie, A. S., and N. J. Middleton. 2006. *Desert Dust in the Global System*: Springer Berlin Heidelberg.

Hamidi, Mehdi, Mohammad Reza Kavianpour, and Yaping Shao. 2013. "Synoptic analysis of dust storms in the Middle East." *Asia-Pacific Journal of Atmospheric Sciences* 49 (3):279–86. doi: 10.1007/s13143-013-0027-9.

Han, Lijian, Atsushi Tsunekawa, Mitsuru Tsubo, and Weiqi Zhou. 2013. "An enhanced dust index for Asian dust detection with MODIS images." *International Journal of Remote Sensing* 34 (19):6484-95.

Hansell, R. A., S. C. Ou, K. N. Liou, J. K. Roskovensky, S. C. Tsay, C. Hsu, and Q. Ji. 2007. "Simultaneous detection/separation of mineral dust and cirrus clouds using MODIS thermal infrared window data." *Geophysical Research Letters* 34 (11). doi: 10.1029/2007gl029388.

Hao, X., and J. J Qu. 2007. "Saharan dust storm detection using moderate resolution imaging spectroradiometer thermal infrared bands." *Journal of Applied Remote Sensing* 1 (013510):013510.

Herman, J. R., P. K. Bhartia, O. Torres, C. Hsu, C. Seftor, and E. Celarier. 1997. "Global distribution of UV-absorbing aerosols from Nimbus 7/TOMS data." *Journal of Geophysical Research: Atmospheres* 102 (D14):16911–22. doi: 10.1029/96jd03680.

Hsu, N. C., S. C. Tsay, M. D. King, and J. R. Herman. 2004. "Aerosol Properties Over Bright-Reflecting Source Regions." *IEEE Transactions on Geoscience and Remote Sensing* 42 (3):557–69. doi: 10.1109/tgrs.2004.824067.

Hsu, N. C., S. C. Tsay, M. D. King, and J. R. Herman. 2006. "Deep blue retrievals of Asian aerosol properties during ACE-Asia." *IEEE Transactions on Geoscience and Remote Sensing* 44 (11):3180-95.

Jafari, R., and M. Malekian. 2015. "Comparison and evaluation of dust detection algorithms using MODIS Aqua/Terra Level 1B data and MODIS/OMI dust products in the Middle East." *International Journal of Remote Sensing* 36 (2):597-617.

Kadioğlu, M., and L. Şaylan. 2001. "Trends of growing degree-days in Turkey." *Water, Air, and Soil Pollution* 126 (1-2):83-96.

Karimi, N., A. Moridnejad, S. Golian, J. M. V. Samani, D. Karimi, and S. Javadi. 2012. "Comparison of dust source identification techniques over land in the Middle East region using MODIS data." *Canadian Journal of Remote Sensing* 38 (5):586-99.

Kaufman, Y. J., D. Tanre, and O. Boucher. 2002. "A satellite view of aerosols in the climate system." *Nature* 419 (6903):215–23. doi: 10.1038/nature01091.

Kaufman, Y. J., A. E. Wald, L. A. Remer, B. Gao, R. Li, and L. Flynn. 1997. "The MODIS 2.1-μm channel-correlation with visible reflectance for use in remote sensing of aerosol." *IEEE Transactions on Geoscience and Remote Sensing* 35 (5):1286–98. doi: 10.1109/36.628795.

Kellogg, C. A., and D. W. Griffin. 2006. "Aerobiology and the global transport of desert dust." *Trends in ecology & evolution* 21 (11):638–44. doi: 10.1016/j.tree.2006.07.004.

Kim, D., M. Chin, H. Yu, T. F. Eck, A. Sinyuk, A. Smirnov, and B. N. Holben. 2011. "Dust optical properties over North Africa and Arabian Peninsula derived from the AERONET dataset." *Atmospheric Chemistry and Physics* 11 (20):10733–41. doi: 10.5194/acp-11-10733-2011.

Kim, Y. J., K. W. Kim, and S. J. Oh. 2001. "Seasonal characteristics of haze observed by continuous visibility monitoring in the urban atmosphere of Kwangju, Korea." *Environmental monitoring and assessment* 70 (1-2):35–46.

Klein, A. G., and A. C. Barnett. 2003. "Validation of daily MODIS snow cover maps of the Upper Rio Grande River Basin for the 2000–2001 snow year." *Remote Sensing of Environment* 86 (2):162-76.

Kutiel, H., and H. Furman. 2003. "Dust storms in the Middle East: sources of origin and their temporal characteristics." *Indoor and Built Environment* 12 (6):419-26.

Laurent, B. 2005. "Simulation of the mineral dust emission frequencies from desert areas of China and Mongolia using an aerodynamic roughness length map derived from the POLDER/ADEOS 1 surface products." *Journal of Geophysical Research* 110 (D18). doi: 10.1029/2004jd005013.

Legrand, M., A. Plana-Fattori, and C. N'doumé. 2001. "Satellite detection of dust using the IR imagery of Meteosat: 1. Infrared difference dust index." *Journal of Geophysical Research: Atmospheres* 106 (D16):18251–74. doi: 10.1029/2000jd900749.

Liu, Y., and R. Liu. 2015. "Climatology of dust storms in northern China and Mongolia: Results from MODIS observations during 2000–2010." *Journal of Geographical Sciences* 25 (11):1298–306. doi: 10.1007/s11442-015-1235-2.

Maghrabi, A., B. Alharbi, and N. Tapper. 2011. "Impact of the March 2009 dust event in Saudi Arabia on aerosol optical properties, meteorological parameters, sky

temperature and emissivity." *Atmospheric Environment* 45 (13):2164–73. doi: 10.1016/j.atmosenv.2011.01.071.

Mélin, F., M. Clerici, G. Zibordi, B. N. Holben, and A. Smirnov. 2010. "Validation of SeaWiFS and MODIS aerosol products with globally distributed AERONET data." *Remote Sensing of Environment* 114 (2):230–50. doi: 10.1016/j.rse.2009.09.003.

Middleton, N. J. 1986. "Dust storms in the Middle East." *Journal of Arid Environments*.

Miller, S. D. 2003. "A consolidated technique for enhancing desert dust storms with MODIS." *Geophysical Research Letters* 30 (20):n/a-n/a. doi: 10.1029/2003gl018279.

Moorthy, K. K., S. S. Babu, S. K. Satheesh, J. Srinivasan, and C. B. S. Dutt. 2007. "Dust absorption over the "Great Indian Desert" inferred using ground-based and satellite remote sensing." *Journal of Geophysical Research* 112 (D9). doi: 10.1029/2006jd007690.

Moridnejad, A., N. Karimi, and P. A-Ariya. 2015. "A new inventory for middle east dust source points." *Environmental monitoring and assessment* 187 (9):582.

Natsagdorj, L., D. Jugder, and Y. S. Chung. 2003. "Analysis of dust storms observed in Mongolia during 1937–1999." *Atmospheric Environment* 37 (9-10):1401–11. doi: 10.1016/s1352-2310(02)01023-3.

O'Loingsigh, T., R. M. Mitchell, S. K. Campbell, N. A. Drake, G. H. McTainsh, N. J. Tapper, and D. L. Dunkerley. 2015. "Correction of dust event frequency from MODIS Quick-Look imagery using in-situ aerosol measurements over the Lake Eyre Basin, Australia." *Remote Sensing of Environment* 169:222–31. doi: 10.1016/j.rse.2015.08.010.

Ozer, P., M. B. O. M. Laghdaf, S. O. M. Lemine, and J. Gassani. 2007. "Estimation of air quality degradation due to Saharan dust at Nouakchott, Mauritania, from horizontal visibility data." *Water, Air, and Soil Pollution* 178 (1):79-87. doi: 10.1007/s11270-006-9152-8.

Parajuli, S. P., Z. Yang, and D. M. Lawrence. 2016. "Diagnostic evaluation of the Community Earth System Model in simulating mineral dust emission with insight into large-scale dust storm mobilization in the Middle East and North Africa (MENA)." *Aeolian Research* 21:21-35.

Pauley, P. M., N. L. Baker, and E. H. Barker. 1996. "An observational Study of the "Interstate 5" Dust Storm Case." *Bulletin of the American Meteorological Society* 77 (4):693-720. doi: 10.1175/1520-0477(1996)077<0693:aosotd>2.0.co;2.

Platnick, S, S. Ackerman, M. D. King, K. G. Meyer, W. P. Menzel, R. E. Holz, B. A. Baum, and P. Yang. 2015. "MODIS atmosphere L2 cloud product (06_L2)." *NASA MODIS Adaptive Processing System, Goddard Space Flight Center, doi* 10.

Prasad, A. K., and R. P. Singh. 2007. "Comparison of MISR-MODIS aerosol optical depth over the Indo-Gangetic basin during the winter and summer seasons (2000–2005)." *Remote Sensing of Environment* 107 (1-2):109–19. doi: 10.1016/j.rse.2006.09.026.

Prospero, J. M., and T. N. Carlson. 1981. "Saharan air outbreaks over the tropical North Atlantic." *Pure and Applied Geophysics PAGEOPH* 119 (3):677–91. doi: 10.1007/bf00878167.

Prospero, J. M., P. Ginoux, O. Torres, S. E. Nicholson, and T. E. Gill. 2002. "Environmental characterization of global sources of atmospheric soil dust identified with the Nimbus 7 Total Ozone Mapping Spectrometer (TOMS) absorbing aerosol product." *Reviews of Geophysics* 40 (1):2-1-2-31. doi: 10.1029/2000RG000095.

Qu, J. J., X. Hao, M. Kafatos, and L. Wang. 2006. "Asian dust storm monitoring combining Terra and Aqua MODIS SRB measurements." *IEEE Geoscience and Remote Sensing Letters* 3 (4):484-6.

Rashki, A., D. G. Kaskaoutis, A. S. Goudie, and R. A. Kahn. 2013. "Dryness of ephemeral lakes and consequences for dust activity: the case of the Hamoun drainage basin, southeastern Iran." *The Science of the total environment* 463-464:552–64. doi: 10.1016/j.scitotenv.2013.06.045.

Remer, L. A, Y. J. Kaufman, D. Tanré, S. Mattoo, D. A. Chu, J. V. Martins, R. R. Li, C. Ichoku, R. C. Levy, and R. G. Kleidman. 2005. "The MODIS aerosol algorithm, products, and validation." *Journal of the Atmospheric Sciences* 62 (4):947-73.

Roskovensky, J. K., and K. N. Liou. 2005. "Differentiating airborne dust from cirrus clouds using MODIS data." *Geophysical Research Letters* 32 (12):n/a-n/a. doi: 10.1029/2005gl022798.

Samadi, M., A. D. Boloorani, S. K. Alavipanah, H. Mohamadi, and M. S. Najafi. 2014. "Global dust Detection Index (GDDI); a new remotely sensed methodology for dust storms detection." *Journal of environmental health science & engineering* 12 (1):20. doi: 10.1186/2052-336x-12-20.

Satheesh, S. K., and K. K. Moorthy. 2005. "Radiative effects of natural aerosols: A review." *Atmospheric Environment* 39 (11):2089-110.

Sayer, A. M., N. C. Hsu, C. Bettenhausen, and M. J. Jeong. 2013. "Validation and uncertainty estimates for MODIS Collection 6 “Deep Blue” aerosol data." *Journal of Geophysical Research: Atmospheres* 118 (14):7864–72. doi: 10.1002/jgrd.50600.

Shahrisvand, M., and M. Akhoondzadeh. 2013. "A COMPARISON OF EMPIRICAL AND INTELIGENT METHODS FOR DUST DETECTION USING MODIS SATELLITE DATA." *ISPRS - International Archives of the Photogrammetry, Remote Sensing and Spatial Information Sciences* XL-1/W3:371–5. doi: 10.5194/isprsarchives-XL-1-W3-371-2013.

Shao, Y. 2008. *Physics and Modelling of Wind Erosion*, *Atmospheric and Oceanographic Sciences Library, 37*. Dordrecht: Springer.

Small, I., J. van der Meer, and R. E. Upshur. 2001. "Acting on an environmental health disaster: the case of the Aral Sea." *Environmental Health Perspectives* 109 (6):547–9.

Smirnov, A., B. N. Holben, T. F. Eck, O. Dubovik, and I. Slutsker. 2000. "Cloud-Screening and Quality Control Algorithms for the AERONET Database." *Remote Sensing of Environment* 73 (3):337–49. doi: 10.1016/s0034-4257(00)00109-7.

Song, Z., J. Wang, and S. Wang. 2007. "Quantitative classification of northeast Asian dust events." *Journal of Geophysical Research: Atmospheres* 112 (D4).

Stanelle, T., I. Bey, T. Raddatz, C. Reick, and I. Tegen. 2014. "Anthropogenically induced changes in twentieth century mineral dust burden and the associated impact on radiative forcing." *Journal of Geophysical Research: Atmospheres* 119, no. 23.

Sun, J., M. Zhang, and T. Liu. 2001. "Spatial and temporal characteristics of dust storms in China and its surrounding regions, 1960-1999: Relations to source area and climate." *Journal of Geophysical Research: Atmospheres* 106 (D10):10325–33. doi: 10.1029/2000jd900665.

Tanaka, T. Y., and M. Chiba. 2006. "A numerical study of the contributions of dust source regions to the global dust budget." *Global and Planetary Change* 52 (1-4):88–104. doi: 10.1016/j.gloplacha.2006.02.002.

Tegen, I., M. Werner, S. P. Harrison, and K. E. Kohfeld. 2004. "Relative importance of climate and land use in determining present and future global soil dust emission." *Geophysical Research Letters* 31 (5):n/a-n/a. doi: 10.1029/2003GL019216.

Tesfaye, M., V. Sivakumar, J. Botai, and G. M. Tsidu. 2011. "Aerosol climatology over South Africa based on 10 years of Multiangle Imaging Spectroradiometer (MISR) data." *Journal of Geophysical Research* 116 (D20). doi: 10.1029/2011jd016023.

Thevenon, F., M. Chiaradia, T. Adatte, C. Hueglin, and J. Poté. 2011. "Ancient versus modern mineral dust transported to high-altitude alpine glaciers evidences saharan sources and atmospheric circulation changes." *Atmospheric Chemistry and Physics Discussions* 11 (1):859–84. doi: 10.5194/acpd-11-859-2011.

Todd, M. C., R. Washington, J. V. Martins, O. Dubovik, G. Lizcano, S. M'bainayel, and S. Engelstaedter. 2007. "Mineral dust emission from the Bodélé Depression, northern Chad, during BoDEx 2005." *Journal of Geophysical Research: Atmospheres* 112 (D6).

Torres, O., P. K. Bhartia, J. R. Herman, Z. Ahmad, and J. Gleason. 1998. "Derivation of aerosol properties from satellite measurements of backscattered ultraviolet radiation: Theoretical basis." *Journal of Geophysical Research: Atmospheres* 103 (D14):17099–110. doi: 10.1029/98jd00900.

Tozer, P., and J. LEYS. 2013. "Dust storms-what do they really cost?" *The Rangeland Journal* 35 (2):131. doi: 10.1071/rj12085.

Varga, G., J. Kovács, and G. Újvári. 2013. "Analysis of Saharan dust intrusions into the Carpathian Basin (Central Europe) over the period of 1979–2011." *Global and Planetary Change* 100:333–42. doi: 10.1016/j.gloplacha.2012.11.007.

Vickery, K. J., F. D. Eckardt, and R. G. Bryant. 2013. "A sub-basin scale dust plume source frequency inventory for southern Africa, 2005-2008." *Geophysical Research Letters* 40 (19):5274–9. doi: 10.1002/grl.50968.

Warner, T. T. 2009. *Desert meteorology*: Cambridge University Press.

Zender, C. S., H. Bian, and D. Newman. 2003. "Mineral Dust Entrainment and Deposition (DEAD) model: Description and 1990s dust climatology." *Journal of Geophysical Research: Atmospheres* 108 (D14):n/a-n/a. doi: 10.1029/2002JD002775.

Zhang, D. D., M. Peart, C. Y. Jim, Y. Q. He, B. S. Li, and J. A. Chen. 2003. "Precipitation chemistry of Lhasa and other remote towns, Tibet." *Atmospheric Environment* 37 (2):231–40. doi: 10.1016/s1352-2310(02)00835-x.

Zhang, X, E. Aguilar, S. Sensoy, H. Melkonyan, U. Tagiyeva, N. Ahmed, N. Kutaladze, F. Rahimzadeh, A. Taghipour, and TH. Hantosh. 2005. "Trends in Middle East climate

extreme indices from 1950 to 2003." Journal of Geophysical Research: Atmospheres 110 (D22).

Zhu, A., V. Ramanathan, F. Li, and D. Kim. 2007. "Dust plumes over the Pacific, Indian, and Atlantic oceans: Climatology and radiative impact." *Journal of Geophysical Research* 112 (D16). doi: 10.1029/2007jd008427.